1   # Towards a Cenozoic History of Atmospheric CO_2

2   ## The Cenozoic CO_2 Proxy Integration Project (CenCO2PIP) Consortium

3

4   **Abstract:** The geological record encodes the relationship between climate and atmospheric
5   carbon dioxide (CO_2) over long and short timescales, as well as potential drivers of evolutionary
6   transitions. However, reconstructing CO_2 beyond direct measurements requires the use of paleo-
7   proxies and herein lies the challenge, as proxies differ in their assumptions, degree of
8   understanding, and even reconstructed values. Here we critically evaluate, categorize, and
9   integrate available proxies to create a high-fidelity and transparently constructed atmospheric
10   CO_2 record spanning the past 66 million years. This provides clearer evidence for higher Earth
11   System Sensitivity in the past and for the role of CO_2 thresholds in biological and cryosphere
12   evolution.

13

14   The contribution of atmospheric CO_2 to Earth's greenhouse effect and the potential for variations
15   in the global carbon cycle to cause climate change has been known for more than a century ([1]),
16   but it was only in 1958 that direct measurements of the concentration of CO_2 in the atmosphere
17   (or molar mixing ratio - the mole fraction of a gas in one mole of air) were systematically
18   collected. Alongside reconstructions of the historical rise in Earth's surface temperature ([2]), this
19   record has become one of the most influential and scientifically valuable environmental time-
20   series, documenting the continuous rise in annual mean CO_2 from 315 parts per million (ppm) in
21   1958 to 419 ppm in 2022 ([3]). Projecting beyond these records to estimate how Earth's climate
22   will respond to further increases in CO_2 requires global climate models ([4]). However, while
23   successful in explaining observed historical climate change ([2]), models leave doubt as to whether
24   global mean temperature will rise linearly as a function of future doubling of CO_2 (i.e., an invariant
25   'climate sensitivity') or whether climate feedbacks will lead to an increasing (or 'state-
26   dependent') sensitivity of climate to CO_2 in the future ([5, 6]).

27   We can turn to the geological record to help constrain models and improve our
28   understanding of non-linearities in the climate system (e.g., [7]), as it documents a variety of global
29   climate changes and critically, climate states warmer than today. Leveraging this record,
30   however, requires the paired quantification of both past atmospheric CO_2 and temperature. In
31   parallel with recent efforts to compile and vet paleo-temperature estimates ([8]), here we focus
32   on paleo-CO_2 estimates. Samples of ancient air can be extracted and analyzed from bubbles
33   preserved in ancient polar ice ([9, 10]), but continuous ice core records currently only extend our
34   knowledge of CO_2 back about 800 thousand years (kyr) (for a compilation, see [11]), with isolated
35   time slices extending to ~2 Ma (million years ago) ([12, 13]). Importantly, at no point during the
36   Pleistocene (2.58 Ma to 11,700 years ago) did CO_2 come close to present-day values (419 ppm,
37   year 2022), with 300 ppm being the highest value measured to date ([14]). In contrast, depending
38   on the extent of future human emissions, atmospheric CO_2 could reach 600–1000 ppm by the
39   year 2100 ([2]). Feedbacks between changing climate and the carbon cycle may also amplify or
40   diminish emissions from surficial carbon reservoirs (e.g., thawing permafrost, adjustments in size
41   and composition of the terrestrial biosphere and marine carbon pool), creating additional
42   uncertainty in future CO_2 projections ([15, 16]). Past changes in CO_2 inherently include the role of
43   these feedbacks, and their study could help reduce uncertainty in Earth system models ([17]).

44   A solid understanding of atmospheric CO_2 variation through geological time is also
45   essential to deciphering and learning from other features of Earth's history. Changes in
46   atmospheric CO_2 and climate are suspected to have caused mass extinctions (e.g., [18, 19]) as well
47   as evolutionary innovations ([20, 21]). During the Cenozoic, long-term declines in CO_2 and
48   associated climate cooling have been proposed as the drivers of changing plant physiology (e.g.,
49   carbon-concentrating mechanisms), species competition and dominance, and associated with
50   this, mammalian evolution. A more refined understanding of past trends in CO_2 is therefore
51   central to understanding how modern species and ecosystems arose and may fare in the future.

52   Extending the CO_2 record beyond the temporally restricted availability of polar ice
53   requires the use of 'proxies'. In essence, a CO_2 proxy could be any biological and/or geochemical
54   property of a fossil or mineral that responds to the concentration of ambient CO_2 when it is
55   formed. Unfortunately, unlike in the case of bubbles of ancient air trapped in polar ice, this
56   response is invariably indirect. The connection between a proxy signal and atmospheric CO_2 is

57 often strongly mediated via biological 'vital effects' (e.g., concentration of or discrimination
58 against certain molecules, elements or isotopes due to physiological processes such as
59 biomineralization, photosynthesis, respiration), may be indirectly connected to the atmosphere
60 via dissolution of carbon in seawater or lakes, may involve isotopic or other chemical
61 fractionation steps, or a combination of these. When preserved in terrestrial or marine
62 sediments, proxy substrates can also be impacted by post-depositional ('diagenetic') processes
63 that must be accounted for. Relationships between proxies and CO_2 are typically calibrated using
64 observations or laboratory experiments; in biological systems, these calibrations are often
65 limited to modern systems (e.g., modern organisms or soils), and applications to the distant past
66 focus on physiologically or physically similar systems preserved in the sediment and rock record
67 (e.g., similar fossil organisms or fossil soils). Most CO_2 proxies also require estimation of one or
68 more additional environmental parameters and hence depend on additional proxy records. The
69 complexity of proxy-enabled paleoclimate reconstructions thus presents a major challenge for
70 creating a self-consistent estimate of atmospheric CO_2 through geological time and requires
71 careful validation.

72   One of the first paleo-CO_2 proxies to be devised was based on the observation that
73 vascular plants typically optimize the density, size, and opening/closing behavior of stomatal
74 pores on their leaf surfaces to ensure sufficient CO_2 uptake while minimizing water loss (e.g., *22*).
75 A count of stomatal frequencies then provides a simple proxy for the CO_2 concentration
76 experienced by the plant (*23*). Changes in ambient CO_2 can also drive a cascade of interrelated
77 effects on photosynthesis, the flux of CO_2 into the leaf (largely determined by stomatal size and
78 density), and the carbon isotopic fractionation during photosynthesis ($\Delta^{13}C$, *22, 23, 24*). While
79 lacking functional stomata, non-vascular plants like liverworts also exhibit isotopic fractionation
80 during photosynthesis, and their $\delta^{13}C$ values are thus similarly controlled by ambient CO_2. The list
81 of terrestrial paleo-CO_2 proxies also includes inorganic carbonate nodules precipitated in ancient
82 soils (i.e., paleosols) as well as sodium carbonate minerals precipitated in continental lacustrine
83 evaporites. While the paleosol proxy uses the carbon isotope composition of carbonate nodules
84 and deconvolves the mixture of atmospheric and soil-respired CO_2 in soil porewaters using
85 models of soil CO_2 (*25, 26*), the nahcolite proxy is based on the CO_2 dependence of sodium
86 carbonate mineral equilibria (*27, 28*). Analogous to non-vascular plants on land, phytoplankton
87 fractionate carbon isotopes during photosynthesis in response to the concentration of dissolved
88 CO_2 in seawater, creating an isotopic signal stored in organic biomolecules that can be retrieved
89 from ocean sediments (*29*). Boron proxies recorded in fossil shells of marine calcifying organisms
90 are related to seawater pH, which in turn can be related back to atmospheric CO_2 (*30, 31*). A
91 detailed discussion of the analytical details, entrained assumptions, and inherent uncertainties
92 of currently available CO_2 proxies, plus summaries of recent advances and opportunities for
93 further validation, is presented in the Supplemental Material and in Table S1.

94   Although each of these proxies has been validated extensively, comparing
95 reconstructions from different proxies often reveals discrepancies. Prior compilations of paleo-
96 CO_2 and explorations of the CO_2-climate linkage already exist (*32-34*), however, those studies
97 applied limited proxy vetting, include CO_2 estimates that predate major innovations in some
98 methods, and use rather basic data interpolation to assess broad CO_2 trends. Earlier CO_2
99 reconstructions are also often insufficiently constrained by ancillary data (e.g., concomitant

100 temperature, isotopic composition of seawater or atmosphere) to be consistent with modern
101 proxy theory, have incomplete or missing uncertainty estimates for CO_2 and/or sample age, and
102 may exhibit fundamental disagreement with other proxies, leaving our current understanding of
103 past CO_2 incomplete.

104   In this study we present the results of a 7-year endeavor by an international consortium
105 of researchers whose collective expertise spans the reconstruction of paleo-CO_2 from all available
106 terrestrial and marine archives. We have jointly created a detailed, open-source database of
107 published paleo-CO_2 estimates including all raw and ancillary data together with associated
108 analytical and computational methods. Each record was vetted and categorized in view of the
109 most recent proxy understanding, with calculations adopting a common methodology including
110 full propagation of uncertainties. We focus our efforts here on the Cenozoic, when the spatial
111 distribution of continents and ocean basins, as well as the structure of marine and terrestrial
112 ecosystems, was similar to the modern, yet profound changes in CO_2 and climate occurred.
113 Identifying the most reliable Cenozoic CO_2 estimates published to date allows us to quantify
114 important physical (e.g., temperature, ice volume) and biological (i.e., physiological, ecosystem)
115 thresholds and tipping points.

116   We structure this investigation as follows: First we summarize the methodology by which
117 we assessed the CO_2 proxies and associated estimates. We then apply these methods to derive
118 a series of paleo CO_2 compilations comprised of data with different levels of quality or
119 confidence, and statistically integrate the 'top-tier' data to create a realization of the Cenozoic
120 variability in atmospheric CO_2. This is followed by a discussion of the climatic implications
121 (including climate sensitivity) of the paleo-CO_2 curve, and a presentation of an evolutionary
122 perspective. We finish with a roadmap for further advances in understanding past changes in
123 atmospheric CO_2.

124

Critical assessment of atmospheric CO_2 proxies

126   The basis of our synthesis is a set of comprehensive data templates documenting all types
127 of proxy data and their corresponding CO_2 estimates (a total of 6,247 data points). The completed
128 data sheets for each study can be accessed as the paleo-CO_2 'Archive' in NOAA's National Climatic
129 Data Center (NCDC). These 'Archive' sheets report all underlying data at face value from the
130 original publications, but their unprecedented level of detail is designed to facilitate critical
131 evaluation and recalculation of each CO_2 estimate.

132   From the 'Archive', published CO_2 estimates were evaluated by teams of experts who are
133 active in validating and applying these proxies, and often included the original authors of the
134 respective data. No new proxy data were collected as part of this effort, but estimates were
135 recalculated where needed and possible, and age models were revised where new evidence was
136 readily accessible. Additionally, CO_2 and age uncertainties were updated, as necessary, to
137 consistently reflect propagated 95% confidence intervals. The vetting criteria are summarized in
138 Supplementary Table S1 and detailed in paleo-CO_2 'Product' sheets. These CO_2 estimates are
139 categorized as follows: 'Category 1' estimates (Fig. 1a, 1,673 data points or ~27% of the original
140 total) are based on data whose uncertainty is fully documented and quantifiable in view of

141 current proxy understanding. 'Category 2' estimates (Fig. 1b, 1,813 data points) contain sources
142 of uncertainty that are not yet fully constrained. These uncertainties vary between proxies and
143 datasets, and include, e.g., insufficient replication, poorly constrained proxy sensitivity to
144 parameters other than CO_2, or extrapolation of calibration curves. 'Category 3' estimates (the
145 residual 2,761 data points or ~44% of the Cenozoic paleo-CO_2 estimates published to date) are
146 either superseded by newer, independently published evaluations from the same raw data, are
147 considered unreliable due to factors such as incomplete supporting datasets that prevent full
148 quantification of uncertainties, or outdated sample preparation methods.

149 Although objective criteria are applied throughout, the vetting process was particularly
150 challenging for the paleosol- and phytoplankton-based proxies because multiple approaches are
151 currently in use for interpreting these proxy data (*35-41*). Given the lack of a universally agreed-
152 upon method, we compare multiple approaches for treating the data of these two proxies
153 whenever possible. For the paleosol proxy, the greatest source of uncertainty is in the estimation
154 of paleo-soil CO_2 concentration derived from respiration. Two different approaches are
155 commonly used to do this. The first method is based on proxy-estimated mean annual rainfall,
156 while the second is based on soil order (i.e., the most general hierarchical level in soil taxonomy,
157 comparable to kingdom in the classification of biological organisms). However, few records in the
158 database allow for a direct comparison between the two approaches. An opportunity for
159 comparison exists with two Eocene records (*37, 42*), where re-calculation using each of the two
160 different methods leads to CO_2 estimates that do not overlap within 95% confidence intervals for
161 most stratigraphic levels (Fig. S6). This implies that the uncertainty in estimating paleo-soil CO_2
162 concentration derived from respiration cannot be fully quantified with either of these
163 approaches. Thus, most paleosol-based CO_2 estimates were designated as Category 2. For the
164 phytoplankton proxy, routinely applied methods differ in how algal cell size and growth rate are
165 accounted for, as well as the assumed sensitivity of algal $\delta^{13}C$ values to aqueous CO_2
166 concentration (see Supplementary Materials for details). Where data are available, we compare
167 both newer and traditional methods, finding that although there are deviations between the
168 resulting CO_2 estimates, they do agree within 95% confidence intervals. We hence assign many
169 phytoplankton CO_2 estimates to Category 1 and present mean CO_2 and uncertainty values that
170 reflect the range of results from the different methods.

171

Towards a Cenozoic history of atmospheric CO_2

173 Our composite Category 1 and 2 realizations of Cenozoic CO_2 (Figs. 1a and b) display much
174 better agreement among proxies than does the 'raw', un-curated collection ('Archive', Fig. 1c).
175 Encouragingly, objective criteria applied to the original data products automatically placed the
176 earlier-reported estimates of 'negative' CO_2, as well as some unusually high values, into Category
177 3, and without subjective intervention to otherwise filter them. We note that the Category 1
178 composite is now largely dominated by marine proxy estimates, with some intervals (e.g., the
179 middle Paleocene, ~63-57 Ma) very sparsely sampled. Furthermore, some intervals (e.g.,
180 Oligocene, Miocene) still exhibit significant differences between proxies; for instance, marine-
181 based CO_2 estimates start high and decline during the Oligocene (~34-23 Ma), whereas plant-
182 based estimates suggest overall lower and constant CO_2 (Fig. 1a). Estimates of global

183   temperature (Fig. 2b) during this time interval are largely invariant, which leaves us with the
184   questions of whether CO_2 and climate were decoupled during this interval, or whether there is a
185   systematic bias in the marine or plant-based CO_2 proxies and/or in the temperature proxies. All
186   proxies become more uncertain further back in time as our knowledge of vital effects in biological
187   proxy carriers, secular changes in the elemental and isotopic composition of ocean and
188   atmosphere, as well as proxy sensitivity to environmental parameters that change along with CO_2
189   (e.g., temperature, rainfall, see Supplementary Materials for details) becomes less certain. In
190   some cases, ancillary constraints and uncertainties are shared across multiple proxies (e.g.,
191   assumed atmospheric $\delta^{13}C$ is common to proxies based on land plant $\delta^{13}C$, leaf gas exchange,
192   and paleosols), creating interdependence of estimates from seemingly independent proxies.
193   More robust paleo-CO_2 reconstruction thus requires not only continued application of all proxies
194   but also replication from different locations.

195   Although some uncertainties and proxy disagreements remain, the much-improved
196   agreement within the vetted paleo-CO_2 compilation gives us confidence that a quantitative
197   reconstruction of Cenozoic CO_2 based on the combined Category 1 data is possible. To do so, we
198   statistically model mean CO_2 values at half-million-year intervals, together with uncertainties in
199   age and proxy CO_2 estimates (Fig. 2a, see Supplementary Materials for details). Our choice of a
200   500-kyr resolution interval reflects a compromise driven by the proxy data compilation. Although
201   parts of the Cenozoic, particularly the Plio-Pleistocene, are sampled at higher temporal
202   resolution, the density of records remains relatively sparse throughout much of the Paleogene (1
203   datum per 190 kyr on average). As a result, the data (and in some cases the underlying age
204   models) are not suited to interpreting higher-frequency (e.g., Milankovitch-scale) variations in
205   atmospheric composition, and we focus here on low-frequency (e.g., multi-million year) trends
206   and transitions. Proxy sampling within some intervals may be biased toward conditions that
207   deviate from the 500-kyr mean (most notably here, the Paleocene-Eocene Thermal Maximum,
208   PETM). We do not attempt to remove this bias but recommend caution in interpreting any
209   features expressed at sub-million-year timescales.

210   This curve (Fig. 2a) allows us to constrain Cenozoic paleo-CO_2 and its uncertainty with
211   greater confidence than earlier efforts. The highest CO_2 values of the past 66 Myr appear during
212   the Early Eocene Climatic Optimum (EECO, ~53-51 Ma), while the lowest values occur during the
213   Pleistocene. In contrast to earlier compilations, which suggested early Cenozoic CO_2
214   concentrations <400 ppm (e.g., *33*), rigorous data vetting and newly published records place early
215   Paleocene mean CO_2 in our reconstruction between 650 and 850 ppm. However, the Paleocene
216   remains data poor, and uncertainty in the curve remains large. Although the Paleocene record is
217   predominantly based on the boron isotope proxy (Fig. 1a), inclusion of other (non-marine) proxy
218   data does influence and refine the reconstruction through this epoch, supporting the value of
219   the multi-proxy approach (Fig. S10). Following the rapid CO_2 rise and fall associated with the
220   PETM at 56 Ma, mean CO_2 steadily rose to peak values of ~1600 ppm around 51 Ma during the
221   EECO. The middle and late Eocene recorded slightly lower values (800-1100 ppm). Mean CO_2
222   dropped to <600 ppm across the Eocene-Oligocene transition (EOT, 33.9 Ma) and reached values
223   that generally fall between ~400 and 200 ppm during the Miocene through Pleistocene, except
224   for a notable increase during the Middle Miocene (~17-15 Ma) to a mean of ~500 ppm.
225   Uncertainty in the mean CO_2 values drops substantially in the Plio-Pleistocene (see also Fig. S11),

226 as expected given a dramatic increase in data density. Our analysis suggests that ~14.5-14 Ma
227 was the last time 500-kyr-mean CO_2 value was as high as the present (Fig. S11), and that all Plio-
228 Pleistocene peak interglacial CO_2 concentrations were exceptionally likely less than those of the
229 modern atmosphere (Fig. S12). In contrast, prior to the Miocene, there is very little support
230 (<2.5% probability) for Cenozoic 500-kyr-mean CO_2 values reaching or falling below pre-industrial
231 levels.

232

233 **Climatic implications of the revised CO_2 curve**

234 **Relationship with global temperature change and climate sensitivity**

235   Our reconstructed Cenozoic CO_2 trends are broadly coherent with those for global
236 temperature as inferred, e.g., from the oxygen isotopic composition ($\delta^{18}O$) of fossil benthic
237 foraminifera shells ([43, 44]) and compilations of global surface temperature ([45]) (Fig. 2b). The
238 Paleocene and Eocene epochs display overall higher temperatures and atmospheric CO_2
239 concentrations as compared to the later Oligocene, Miocene, and Pliocene - consistent with a
240 predominantly greenhouse-gas regulated global energy budget. More specifically, the slow rise
241 and subsequent fall of CO_2 over the course of the Paleocene and Eocene are mirrored by global
242 temperatures, just as a transient Miocene CO_2 rise coincides with a period of warming at the
243 Miocene Climatic Optimum (MCO). The EOT is identifiable in both the CO_2 and temperature
244 records, despite the smoothing introduced by the curve fitting and 500-kyr binning interval.

245   Despite this overall agreement, rates and timing of CO_2 vs. temperature changes in the
246 two records are not always synchronized (Fig. 2a,b). For example, CO_2 appears broadly static or
247 even rising during the late Eocene (37-34 Ma) and late Miocene (11-5 Ma) despite global cooling
248 (see also [46]) at these times. Conversely, decreasing CO_2 during the early Oligocene corresponds
249 with relatively stable global temperatures (Fig. 2b, but see also [47, 48]) and ice volume (Fig. 2c) at
250 that time. We note that the reconstructed Oligocene CO_2 decrease is driven by the contribution
251 of marine proxies to the composite curve, whereas estimates from leaf gas exchange proxies are
252 low and broadly static (Fig. 1c), a discrepancy that cannot be resolved without further
253 experimentation and data collection. We caution that, even at the 500-kyr resolution of our
254 study, the relative timing of CO_2 and temperature change might be unresolved in poorly sampled
255 intervals (i.e., middle Paleocene), but should be well resolved during more recent, well sampled
256 intervals (i.e., late Miocene through present, Fig. S8). Is the occasional divergence of temperature
257 and CO_2 change evidence for occasional disconnects between CO_2 forcing and climate response?
258 Although one might posit bias in the CO_2 reconstruction, the strength of our multiproxy approach
259 is the reduced likelihood that multiple proxies exhibit common bias during particular periods of
260 the Cenozoic. We suggest that some cases of divergence between temperature and CO_2 could
261 reflect non-CO_2 effects on climate (e.g., changes in paleogeography affecting ocean circulation,
262 albedo and heat transport, [49]), or the temperature reconstructions used herein could be biased
263 by non-thermal influences (e.g., uncertain elemental and isotopic composition of paleo-
264 seawater, physiological or pH effects on proxies, [48, 50]).

265   Our updated CO_2 curve, in conjunction with existing global temperature reconstructions,
266 gives us the opportunity to reassess how climate sensitivity might have evolved through the

Cenozoic. The most commonly reported form of climate sensitivity is equilibrium climate sensitivity (ECS), which focuses on fast feedback processes (e.g., clouds, lapse rate, snow, sea ice) and is therefore best suited for predicting present-day warming (~3°C for a doubling of CO_2 above the pre-industrial condition, *2*). Because the average temporal resolution of our CO_2 database is coarser than 1000 years, we cannot estimate ECS directly. Instead, our data are most appropriate for interpreting an Earth System Sensitivity (ESS$_{[CO2]}$, following the taxonomy of *51*) – the combination of short-term climate responses to doubling CO_2 plus the effects of slower, geological feedback loops such as the growth and decay of continental ice sheets. We compare our reconstructed 500-kyr-mean CO_2 values with two different estimates of global surface temperature. We apply the same Bayesian inversion model used in the CO_2 reconstruction to derive 500-kyr-mean surface temperatures from the benthic foraminiferal $\delta^{18}O$ compilation of Ref. (*43*), which we convert to temperatures using the methodology of Ref. (*44*) (Fig. 2b). In addition, we pair a set of multiproxy global surface temperature estimates for eight Cenozoic time intervals (Fig. 2b, *45*) with posterior CO_2 estimates from time bins corresponding to each interval. The two temperature reconstructions are broadly similar, although the benthic record suggests relatively higher temperatures during the hothouse climate of the Paleocene and Eocene, whereas the multiproxy reconstruction is elevated relative to the benthic record during the Oligocene and Neogene.

The co-evolution of atmospheric CO_2 and global mean surface temperature (GMST) over the Cenozoic is shown in Fig. 3. Because CO_2 is on a log scale, the slopes of lines connecting two adjacent points in time reflect the average intervening ESS$_{[CO2]}$. Benthic $\delta^{18}O$-derived temperatures suggest early Paleocene warming occurs with a very high ESS$_{[CO2]}$ (>8°C per CO_2 doubling), although CO_2 uncertainties are large during this time interval. ESS$_{[CO2]}$ steadily declines towards the peak of Cenozoic warmth ~50 Ma, then steepens again to ~8°C per CO_2 doubling for much of the cooling through to the EOT at ~34 Ma. In contrast, the multiproxy global temperature record suggests a lower ESS$_{[CO2]}$ of ~5°C between the early Eocene and earliest Oligocene. During the Oligocene and early part of the Miocene, both temperature records imply a near-zero ESS$_{[CO2]}$, i.e., CO_2 values appear to decline with no appreciable global cooling. ESS$_{[CO2]}$ implied by both temperature reconstructions steepens again from the middle Miocene (~16 Ma) to present, averaging 8°C per CO_2 doubling over the past 10 Myr.

An alternative perspective on early Cenozoic climate forcing was introduced by Ref. (*44*), who hypothesized that all pre-Oligocene climate change was the response of direct and indirect CO_2 radiative forcing plus long-term change in solar output (i.e., constant albedo). Given this, they converted Paleocene and Eocene benthic $\delta^{18}O$-derived GMST to estimates of CO_2 change required to explain the temperature record. Our reconstruction offers a direct test of this hypothesis, and although it compares well with the $\delta^{18}O$ approach of Ref. (*44*) throughout much of the early Cenozoic, our curve suggests that the late Eocene decline in CO_2 was less severe than expected under the constant albedo assumption (Fig. S13). This result is consistent with a growing contribution of glacier and sea ice albedo effects (e.g., *52, 53*) and the opening of Southern Ocean gateways (e.g., *54*) to climate cooling preceding the Eocene-Oligocene boundary.

308   In summary, the Cenozoic compilation confirms a strong link between CO_2 and GMST
309   across timescales from 500 kyr to tens of Myr, with $ESS_{[CO2]}$ generally within the range of 5-8°C –
310   patterns consistent with most prior work (*32-34, 45, 51, 55-60*), and considerably higher than the
311   present-day ECS of ~3°C. Both temperature reconstructions imply relatively high $ESS_{[CO2]}$ values
312   during the last 10 Myr of the Cenozoic, when global ice volumes were highest. This agrees with
313   expectations of an amplified $ESS_{[CO2]}$ due to the ice-albedo feedback (*61*). However, even during
314   times with little-to-no ice (Paleocene to early Eocene), we find elevated values of $ESS_{[CO2]}$
315   (approaching or exceeding 5°C per CO_2 doubling). This implies that fast, non-ice feedbacks, such
316   as clouds or non-CO_2 greenhouse gases (*60, 62-65*) were probably stronger in the early Paleogene
317   than they are in the present-day climate system (see also *5*). The Oligocene to early Miocene is
318   the most enigmatic interval, with an apparent decrease in CO_2 despite relatively stable
319   temperature, implying near zero $ESS_{[CO2]}$. It should be noted that this is one interval where
320   different CO_2 proxies disagree on CO_2 change (Fig. 1a), with relatively stable values from plants
321   but a decline in values from alkenones. More work is needed to confirm these CO_2 and
322   temperature findings, but if these estimates are correct, this could partly reflect transition from
323   a climate state too cold to support the strong fast feedbacks (e.g., clouds) of the early Eocene (*5*),
324   but not cold enough to generate strong ice-albedo feedback. Tectonic changes in the
325   arrangement of continents and the opening of critical ocean gateways may also be confounding
326   derivation of $ESS_{[CO2]}$ at that time (e.g., *49, 54*).

327   **Relationship with the evolution of the cryosphere**

328   Our composite CO_2 record also enables reexamination of the evolution of Earth's
329   cryosphere (Fig. 2c) in relation to CO_2 radiative forcing. We use the sea level estimation of Ref.
330   (*66*) for this comparison because it covers the entire Cenozoic and is somewhat independent of
331   the benthic $\delta^{18}O$ stack (*43*) used for the GMST derivation in Fig. 2b and also of the more recent
332   sea level reconstruction of Ref. (*67*). Although there are significant differences between the two
333   sea level estimates, the main features discussed herein are broadly consistent between them.
334   The establishment of a permanent, continent-wide Antarctic ice shield at the EOT (~34 Ma)
335   comes at the end of a ~10-Myr period of generally slowly decreasing CO_2. There is evidence for
336   isolated, unstable Antarctic glaciers at various points over the 10-Myr interval prior to the EOT
337   (*50, 53, 66, 68*), which is consistent with the increasing paleogeographic isolation of Antarctica
338   and Southern Ocean cooling (*54*), and CO_2 may have been sufficiently low to enable the repeated
339   crossing of a glaciation threshold by periodic orbital forcing. Tectonic cooling of Antarctica would
340   have progressively raised the CO_2 glaciation threshold, which has been modeled to be within 560-
341   920 ppm (*69, 70*). Our composite CO_2 record allows us to further assess this glaciation threshold
342   but requires determining the point during glacial inception when strong positive feedbacks (e.g.,
343   ice-albedo and ice sheet elevation) commenced and ice sheet growth accelerated (*71*). Using the
344   sea level curve of Ref. (*66*), we determine this point as 33.75 ±0.25 Ma, where our composite CO_2
345   record suggests 719 $^{+180}_{-152}$ ppm (95% CIs). Once established, the land-based Antarctic ice sheet
346   likely persisted for the remainder of the Cenozoic, although significant retreat of land-based ice
347   has been modeled (30-36 m sea level equivalent, *72*) and estimated from proxies (Fig. 2c) for the
348   Miocene Climatic Optimum (MCO). 500-kyr-mean CO_2 values increased to ~500 ppm during the
349   MCO (Figs. 2a, S10), and benthic foraminiferal $\delta^{18}O$ (Fig. 2b, *43*) and clumped isotopes (*50*)

350 indicate warming. While the stability of the land-based Antarctic ice sheet depends on many
351 factors in addition to CO_2-induced global warming (e.g., hysteresis ([73]), bed topography ([74])),
352 our composite record indicates that significant retreat of land-based ice did not occur below 441-
353 480 ppm (2.5-50 percentiles), and some land-based ice may have persisted up to 563 ppm (97.5
354 percentile) during the MCO. Excepting the MCO, atmospheric CO_2 has remained below our
355 current value of 419 ppm since the late Oligocene (Figs. 2a, S10), with relatively small sea-level
356 variations (up to ~20m, Fig. 2c and [67]) being driven by orbitally-forced melting of the marine-
357 based ice sheet (e.g., [72, 75]). Finally, at ~2.7 Ma, the transition to intensified northern
358 hemisphere glaciation and orbitally-driven glacial cycles coincided with CO_2 values that began
359 decreasing after a relative high during the Pliocene (Fig. 2a).

360

361 **Evolutionary implications of the revised CO_2 curve**

362 While geologic trends in terrestrial floral and faunal habitat ranges (e.g., [76, 77]) and diversity
363 (e.g., [78, 79, 80]) are largely thought to be controlled by temperature and associated climate
364 patterns, atmospheric CO_2 has been hypothesized to drive the evolution of biological carbon
365 concentrating mechanisms and their subsequent diversification in terrestrial plants (CCMs, Fig.
366 2d, [81, 82]). Our realization of how atmospheric CO_2 has varied through the Cenozoic allows us to
367 re-examine this hypothesis. The two primary CCMs in terrestrial plants are the crassulacean acid
368 metabolism (CAM) and C_4 photosynthetic syndromes. CCMs in terrestrial C_4 and CAM plants
369 confer competitive advantages over the ancestral C_3 pathway under higher growing season
370 temperatures, low rainfall, and lower atmospheric CO_2. As a result, C_4 photosynthesis contributes
371 about 23% of today's global terrestrial gross primary production (GPP, [83]).

372 Plant clades with the C_4 pathway first emerged in the early Oligocene ([84, 85]), yet did not
373 expand to ecological significance until the late Miocene (i.e., <5% GPP before ~10 Ma, Fig. 2d, [86,
374 [87, 88]). CAM plants (e.g., cacti, ice plants, agaves, and some orchids) underwent significant
375 diversification events around the late Oligocene and late Miocene ([89-91]). Taken together, two
376 general biological thresholds emerge based on our CO_2 record: (1) All known origins of C_4 plants
377 occurred when atmospheric CO_2 was lower than ~550 ppm (i.e., after 32 Ma, Fig. 2a,d, [84]), which
378 is in agreement with theoretical predictions ([92, 93]). (2) All major Cenozoic CAM diversification
379 events coincided with intervals when CO_2 was lower than ~430 ppm (i.e., after 27 Ma, [89, 90]).
380 Our record is thus consistent with decreasing atmospheric CO_2 (< 550 ppm) being a critical
381 threshold for the Cenozoic origin, diversification, and expansion of C_4 and CAM plants within
382 grasslands, arid habitats (such as deserts), and habits (such as epiphytes), and provides strong
383 data support for previous hypotheses ([20, 84, 86, 88, 89, 92, 94, 95]). Importantly, following their
384 origin in the early Oligocene, C_4 plants did not immediately proliferate. By ~24 to ~18 Ma, open
385 habitat grasslands are evident on most continents ([96]), yet widespread dispersal of C_4 plants was
386 delayed until the late Miocene, and without any apparent decline in CO_2 (Fig. 2d). Therefore, the
387 rise of C_4 plants to their dominance in many tropical and subtropical ecosystems was likely driven
388 (and maintained today) by other factors such as fire, seasonality of rainfall, and herbivory (i.e.,
389 grazing that keeps landscapes open) ([97, 98]). The temporal evolution of these factors warrants
390 further study as we move towards a future where CO_2 may rise above the 550-ppm threshold
391 that was key to the origin, taxonomic diversification, and spread of C_4 plants.

392

393   Terrestrial mammals evolved and adapted to the changing and more open floral
394   ecosystems of the late Cenozoic (*99-101*), and are thus indirectly linked to the 550-ppm
395   atmospheric CO_2 threshold discovered herein. In particular, dental wear patterns (such as the
396   shape of the chewing surface of a tooth, i.e., mesowear) and tooth morphology, such as crown
397   height, reflect an increasingly abrasive and tough diet (*102, 103*), and can be traced across many
398   herbivore lineages during this period. For instance, mesowear in North American Equidae (horses
399   and their ancestors, Fig. 2d) began to increase in the late Eocene, and steadily continued into the
400   Quaternary. Similarly, equids evolved high-crowned (hypsodont) teeth in the Miocene (*103-105*),
401   and their body size increased to accommodate higher intake of more abrasive, grassy vegetation
402   (Fig. 2d).

403   Evolutionary trends are a little less clear in the ocean, because marine algal CCMs are
404   ubiquitous and diverse in form (*106*) and are believed to have an ancient origin. Moreover, the
405   large spatial and seasonal variance of dissolved CO_2 in the surface ocean (as compared to the
406   relatively uniform seasonal and spatial concentration of CO_2 in the air) may somewhat decouple
407   their evolution from geologic trends in atmospheric CO_2. Evidence exists that marine algae, and
408   in particular the coccolithophores (i.e., the source of the alkenone biomarkers), express CCMs to
409   greater extent when CO_2 is lower (e.g., *107, 108, 109*), with estimates of cellular carbon fluxes
410   suggesting enhanced CCM activity in coccolithophores began ~7-5 Ma (*110*). However, our
411   revised CO_2 curve displays mean atmospheric CO_2 broadly constant at 300-350 ppm since at least
412   ~14 Ma (Figs. 2a, S10), suggesting that increased CCM activity may reflect other proximal triggers,
413   perhaps involving changes in ocean circulation and nutrient supply.

414

Perspectives and opportunities for further advances

416   Our community-assessed composite CO_2 record and statistically modelled time-averaged
417   CO_2 curve exhibit greater clarity in the Cenozoic evolution of CO_2 and its relationship with climate
418   than was possible in previous compilations, and furthermore highlight the value of cross-
419   disciplinary collaboration and community building. Generating a paleo-CO_2 record with even
420   greater confidence requires targeted efforts using multiple proxies to fill in data gaps, higher
421   resolution and replication from multiple locations, and novel approaches to resolve remaining
422   differences between CO_2 proxy estimates. Specifically: although the number and diversity of
423   paleo-CO_2 proxy records continues to grow, data remain relatively sparse during several key parts
424   of the Cenozoic record (e.g., middle Paleocene, Oligocene). Moreover, records from the
425   Paleocene and Eocene are dominated by estimates from the boron isotope proxy, increasing
426   potential for bias. Targeted efforts are hence needed to expand the number and diversity of data
427   through these intervals and to refine multi-proxy reconstructions. Secondly, despite substantial
428   progress, there remains a lack of consensus regarding the identity and/or quantification of some
429   of the factors underlying each of the proxy systems analyzed here. New experimental and
430   calibration studies, particularly those that isolate and quantify specific mechanistic responses
431   and/or their interactions, need to be undertaken in order to reduce potential biases and
432   uncertainty for each method. For instance, the emerging fields of genomics, evolutionary and
433   developmental biology, and proteomics provide exciting new opportunities for improving and

434 understanding paleo-proxy systematics. Thirdly, and associated with improved experimental
435 quantification, refining our theoretical and mechanistic understanding of how proxies are
436 encoded will allow us to create explicit and self-consistent representations of the processes
437 involved. The development of proxy system forward models provides a promising leap in this
438 direction (e.g., *111*). Bayesian statistical methods can then enable the full suite of models and
439 data to be integrated and constrain the range of environmental conditions, including
440 atmospheric CO_2 and other variables that are consistent with the multiproxy data (*112, 113*).
441 Finally, development of new proxies is also a realistic and desirable aim. For instance, while this
442 study focuses on more established proxies, new proxies such as coccolith calcite stable isotopes
443 (*114*) and mammalian bone and teeth oxygen-17 anomalies (*115*) show promising results for
444 reconstructing paleo-CO_2, but perhaps require further validation before they can be assessed
445 with confidence.

446   Proxies and proxy-based reconstructions of how atmospheric CO_2 has varied through
447 deep time have improved immeasurably over the past few decades. While they will never allow
448 us to reconstruct past CO_2 with the same fidelity as direct air measurement, our study shows how
449 community-based consensus assessment, together with a critical reanalysis of proxy models and
450 assumptions, can progressively move us towards a quantitative history of atmospheric CO_2 for
451 geological time.

452
453

References and Notes

1. S. Arrhenius, *Philosophical Magazine* **41**, 237 (1896).
2. IPCC, *Climate Change 2021: The Physical Science Basis. Contribution of Working Group I to the Sixth Assessment Report of the Intergovernmental Panel on Climate Change*. V. Masson-Delmotte, P. Zhai, A. Pirani, S. L. Connors, C. Péan, S. Berger *et al.*, Eds., (Cambridge University Press, Cambridge, United Kingdom and New York, NY, USA, 2021).
3. P. Tans, R. Keeling, NOAA/ESRL, Ed. (NOAA/ESRL, www.esrl.noaa.gov/gmd/ccgg/trends/, 2023).
4. K. E. Taylor, R. J. Stouffer, G. A. Meehl, *Bulletin of the American Meteorological Society* **93**, 485 (2012/04/01, 2011).
5. R. Caballero, M. Huber, *Proceedings of the National Academy of Sciences USA* **110**, 14162 (August 5, 2013, 2013).
6. J. Zhu, C. J. Poulsen, *Geophysical Research Letters* **47**, e2020GL089143 (2020/09/28, 2020).
7. J. Zhu, C. J. Poulsen, B. L. Otto-Bliesner, *Nature Climate Change* **10**, 378 (2020/05/01, 2020).
8. E. J. Judd, J. E. Tierney, B. T. Huber, S. L. Wing, D. J. Lunt, H. L. Ford *et al.*, *Scientific Data* **9**, 753 (2022/12/06, 2022).
9. R. J. Delmas, J.-M. Ascencio, M. Legrand, *Nature* **284**, 155 (1980).
10. A. Neftel, H. Oeschger, J. Schwander, B. Stauffer, R. Zumbrunn, *Nature* **295**, 220 (1982).
11. B. Bereiter, S. Eggleston, J. Schmitt, C. Nehrbass-Ahles, T. F. Stocker, H. Fischer *et al.*, *Geophysical Research Letters* **42**, 542 (2015).
12. Y. Yan, M. L. Bender, E. J. Brook, H. M. Clifford, P. C. Kemeny, A. V. Kurbatov *et al.*, *Nature* **574**, 663 (2019/10/01, 2019).
13. J. A. Higgins, A. V. Kurbatov, N. E. Spaulding, E. Brook, D. S. Introne, L. M. Chimiak *et al.*, *Proceedings of the National Academy of Sciences* **112**, 6887 (June 2, 2015, 2015).
14. C. Nehrbass-Ahles, J. Shin, J. Schmitt, B. Bereiter, F. Joos, A. Schilt *et al.*, *Science* **369**, 1000 (2020).
15. C. Le Quéré, M. R. Raupach, J. G. Canadell, G. Marland, et al., *Nature Geosci* **2**, 831 (2009).
16. P. Friedlingstein, M. O'Sullivan, M. W. Jones, R. M. Andrew, L. Gregor, J. Hauck *et al.*, *Earth Syst. Sci. Data* **14**, 4811 (2022).
17. P. Valdes, *Nat. Geosci.* **4**, 414 (2011/07/01, 2011).
18. W. Kiessling, M. Aberhan, L. Villier, *Nature Geosci* **1**, 527 (2008).
19. J. L. Payne, A. M. Bush, N. A. Heim, M. L. Knope, D. J. McCauley, *Science* **353**, 1284 (2016).
20. E. J. Edwards, C. P. Osborne, C. A. Strömberg, S. A. Smith, W. J. Bond, P. A. Christin *et al.*, *Science* **328**, 587 (Apr 30, 2010).
21. F. A. McInerney, S. L. Wing, *Annual Review of Earth and Planetary Sciences* **39**, 489 (2011/05/30, 2011).
22. W. Konrad, D. L. Royer, P. J. Franks, A. Roth-Nebelsick, *Geological Journal*, (2020/03/18, 2020).

498   23.   J. C. McElwain, M. Steinthorsdottir, *Plant Physiology* **174**, 650 (2017).

499   24.   B. A. Schubert, A. H. Jahren, *Geochim. Cosmochim. Acta* **96**, 29 (2012).

500   25.   T. E. Cerling, *Am. J. Sci.* **291**, 377 (1991).

501   26.   D. O. Breecker, *Geochemistry, Geophysics, Geosystems* **14**, 3210 (2013/08/01, 2013).

502   27.   E. A. Jagniecki, T. K. Lowenstein, D. M. Jenkins, R. V. Demicco, *Geology* **43**, 1075
503   (December 1, 2015, 2015).

504   28.   T. K. Lowenstein, R. V. Demicco, *Science* **313**, 1928 (2006).

505   29.   M. Pagani, in *Treatise on Geochemistry (Second Edition),* H. D. Holland, K. K. Turekian,
506   Eds. (Elsevier, Oxford, 2014), pp. 361-378.

507   30.   B. Hönisch, S. M. Eggins, L. L. Haynes, K. A. Allen, K. Holland, K. Lorbacher, *Boron proxies*
508   *in Paleoceanography and Paleoclimatology*. Analytical Methods in Earth and
509   Environmental Science (John Wiley & Sons, Ltd., 2019).

510   31.   J. W. B. Rae, in *Boron Isotopes: The Fifth Element,* H. Marschall, G. Foster, Eds. (Springer
511   International Publishing, Cham, 2018), pp. 107-143.

512   32.   D. J. Beerling, D. L. Royer, *Nat. Geosci.* **4**, 418 (2011).

513   33.   G. L. Foster, D. L. Royer, D. J. Lunt, *Nature Communications* **8**, 14845 (04/04/online,
514   2017).

515   34.   J. W. B. Rae, Y. G. Zhang, X. Liu, G. L. Foster, H. M. Stoll, R. D. M. Whiteford, *Annual*
516   *Review of Earth and Planetary Sciences* **49**, 609 (2021).

517   35.   S. Ji, J. Nie, A. Lechler, K. W. Huntington, E. O. Heitmann, D. O. Breecker, *Earth and*
518   *Planetary Science Letters* **499**, 134 (2018/10/01/, 2018).

519   36.   J. Da, Y. G. Zhang, G. Li, X. Meng, J. Ji, *Nature Communications* **10**, 4342 (2019/09/25,
520   2019).

521   37.   E. Hyland, N. D. Sheldon, M. Fan, *GSA Bulletin* **125**, 1338 (2013).

522   38.   J. Henderiks, M. Pagani, *Paleoceanography* **22**, (2007).

523   39.   S. R. Phelps, G. M. M. Hennon, S. T. Dyhrman, M. D. Hernández Limón, O. M.
524   Williamson, P. J. Polissar, *Geochemistry, Geophysics, Geosystems* **22**, e2021GC009657
525   (2021/07/01, 2021).

526   40.   H. M. Stoll, J. Guitian, I. Hernandez-Almeida, L. M. Mejia, S. Phelps, P. Polissar *et al.*,
527   *Quaternary Science Reviews* **208**, 1 (2019/03/15/, 2019).

528   41.   Y. G. Zhang, J. Henderiks, X. Liu, *Geochimica et Cosmochimica Acta* **281**, 118
529   (2020/07/15/, 2020).

530   42.   E. G. Hyland, N. D. Sheldon, *Palaeogeography, Palaeoclimatology, Palaeoecology* **369**,
531   125 (2013).

532   43.   T. Westerhold, N. Marwan, A. J. Drury, D. Liebrand, C. Agnini, E. Anagnostou *et al.*,
533   *Science* **369**, 1383 (2020).

534   44.   J. Hansen, M. Sato, G. Russell, P. Kharecha, *Philosophical Transactions of the Royal*
535   *Society A: Mathematical, Physical and Engineering Sciences* **371**, 20120294 (2013/10/28,
536   2013).

537   45.   S. J. Ring, S. G. Mutz, T. A. Ehlers, *Paleoceanography and Paleoclimatology* **37**,
538   e2021PA004364 (2022/12/01, 2022).

539   46.   T. D. Herbert, K. T. Lawrence, A. Tzanova, L. C. Peterson, R. Caballero-Gill, C. S. Kelly,
540   *Nature Geosci* **9**, 843 (11//print, 2016).

541 47. D. E. Gaskell, M. Huber, L. O'Brien Charlotte, N. Inglis Gordon, R. P. Acosta, J. Poulsen
542 Christopher *et al.*, *Proceedings of the National Academy of Sciences* **119**, e2111332119
543 (2022/03/15, 2022).
544 48. C. L. O'Brien, M. Huber, E. Thomas, M. Pagani, J. R. Super, L. E. Elder *et al.*, *Proceedings*
545 *of the National Academy of Sciences* **117**, 25302 (2020).
546 49. D. J. Lunt, A. Farnsworth, C. Loptson, G. L. Foster, P. Markwick, C. L. O'Brien *et al.*, *Clim.*
547 *Past* **12**, 1181 (2016).
548 50. A. N. Meckler, P. F. Sexton, A. M. Piasecki, T. J. Leutert, J. Marquardt, M. Ziegler *et al.*,
549 *Science* **377**, 86 (2022/07/01, 2022).
550 51. PALEOSENS-project-members, *Nature* **419**, 683 (2012).
551 52. A. Tripati, D. Darby, *Nature Communications* **9**, 1038 (2018/03/12, 2018).
552 53. H. D. Scher, S. M. Bohaty, B. W. Smith, G. H. Munn, *Paleoceanography* **29**, 628
553 (2014/06/01, 2014).
554 54. I. Sauermilch, J. M. Whittaker, A. Klocker, D. R. Munday, K. Hochmuth, P. K. Bijl *et al.*,
555 *Nature Communications* **12**, 6465 (2021/11/09, 2021).
556 55. D. L. Royer, *Annual Review of Earth and Planetary Sciences* **44**, 277 (2016).
557 56. R. M. Brown, T. B. Chalk, A. J. Crocker, P. A. Wilson, G. L. Foster, *Nat. Geosci.* **15**, 664
558 (2022/08/01, 2022).
559 57. T. E. Wong, Y. Cui, D. L. Royer, K. Keller, *Nature Communications* **12**, 3173 (2021/05/26,
560 2021).
561 58. D. L. Royer, M. Pagani, D. J. Beerling, *Geobiology* **10**, 298 (2012/07/01, 2012).
562 59. J. E. Tierney, J. Zhu, M. Li, A. Ridgwell, G. J. Hakim, C. J. Poulsen *et al.*, *Proceedings of the*
563 *National Academy of Sciences* **119**, e2205326119 (2022/10/18, 2022).
564 60. E. Anagnostou, E. H. John, T. L. Babila, P. F. Sexton, A. Ridgwell, D. J. Lunt *et al.*, *Nature*
565 *Communications* **11**, 4436 (2020/09/07, 2020).
566 61. J. Hansen, M. Sato, P. Kharecha, D. Beerling, R. Berner, V. Masson-Delmotte *et al.*, *Open*
567 *Atm. Sci. J.* **2**, 217 (2008).
568 62. J. T. Kiehl, C. A. Shields, *Philosophical Transactions of the Royal Society A* **371**, 20130093
569 (October 28, 2013, 2013).
570 63. J. Zhu, C. J. Poulsen, J. E. Tierney, *Science Advances* **5**, eaax1874 (2019).
571 64. D. J. Beerling, A. Fox, D. S. Stevenson, P. J. Valdes, *Proceedings of the National Academy*
572 *of Sciences* **108**, 9770 (2011/06/14, 2011).
573 65. T. Schneider, C. M. Kaul, K. G. Pressel, *Nat. Geosci.* **12**, 163 (2019/03/01, 2019).
574 66. K. G. Miller, J. V. Browning, W. J. Schmelz, R. E. Kopp, G. S. Mountain, J. D. Wright,
575 *Science Advances* **6**, eaaz1346 (2020).
576 67. E. J. Rohling, J. Yu, D. Heslop, G. L. Foster, B. Opdyke, A. P. Roberts, *Science Advances* **7**,
577 eabf5326 (2021).
578 68. M. J. Henehan, K. M. Edgar, G. L. Foster, D. E. Penman, P. M. Hull, R. Greenop *et al.*,
579 *Paleoceanography and Paleoclimatology* **35**, e2019PA003713 (2020/06/01, 2020).
580 69. E. Gasson, D. J. Lunt, R. DeConto, A. Goldner, M. Heinemann, M. Huber *et al.*, *Clim. Past*
581 **10**, 451 (2014).
582 70. R. M. DeConto, D. Pollard, P. A. Wilson, H. Palike, C. H. Lear, M. Pagani, *Nature* **455**, 652
583 (2008).
584 71. R. M. DeConto, D. Pollard, *Nature* **421**, 245 (2003).

585 72. E. Gasson, R. M. DeConto, D. Pollard, R. H. Levy, *Proceedings of the National Academy of*
586   *Sciences* **113**, 3459 (2016/03/29, 2016).
587 73. D. Pollard, R. M. DeConto, *Glob. Planet. Change* **45**, 9 (2005/02/01/, 2005).
588 74. G. J. G. Paxman, E. G. W. Gasson, S. S. R. Jamieson, M. J. Bentley, F. Ferraccioli,
589   *Geophysical Research Letters* **47**, e2020GL090003 (2020/10/28, 2020).
590 75. J. J. Fürst, G. Durand, F. Gillet-Chaulet, L. Tavard, M. Rankl, M. Braun *et al.*, *Nature*
591   *Climate Change* **6**, 479 (2016/05/01, 2016).
592 76. J. C. McElwain, *Annual Review of Plant Biology* **69**, 761 (2018/04/29, 2018).
593 77. S.-M. Popescu, J.-P. Suc, S. Fauquette, M. Bessedik, G. Jiménez-Moreno, C. Robin *et al.*,
594   *Journal of Biogeography* **48**, 2771 (2021/11/01, 2021).
595 78. C. Jaramillo, M. J. Rueda, G. Mora, *Science* **311**, 1893 (Mar 31, 2006).
596 79. J. Y. Lim, H. Huang, A. Farnsworth, D. J. Lunt, W. J. Baker, R. J. Morley *et al.*, *Global*
597   *Ecology and Biogeography* **31**, 425 (2022/03/01, 2022).
598 80. A. Graham, *Am J Bot* **98**, 336 (Mar, 2011).
599 81. J. R. Ehleringer, R. K. Monson, *Annual Review of Ecology and Systematics* **24**, 411 (1993).
600 82. H. Griffiths, in *Vascular plants as epiphytes,* U. Lüttge, Ed. (Springer, Berlin, 1989), pp.
601   42–86.
602 83. C. J. Still, J. A. Berry, G. J. Collatz, R. S. DeFries, *Glob. Biogeochem. Cycle* **17**, 6
603   (2003/03/01, 2003).
604 84. P.-A. Christin, G. Besnard, E. Samaritani, M. R. Duvall, T. R. Hodkinson, V. Savolainen *et*
605   *al.*, *Current Biology* **18**, 37 (2008/01/08/, 2008).
606 85. A. Vicentini, J. C. Barber, S. S. Aliscioni, L. M. Giussani, E. A. Kellogg, *Glob. Change Biol.*
607   **14**, 2963 (2008/12/01, 2008).
608 86. P. J. Polissar, C. Rose, K. T. Uno, S. R. Phelps, P. deMenocal, *Nat. Geosci.* **12**, 657
609   (2019/08/01, 2019).
610 87. L. Tauxe, S. J. Feakins, *Paleoceanography and Paleoclimatology* **35**, e2020PA003857
611   (2020/07/01, 2020).
612 88. T. E. Cerling, J. M. Harris, B. J. MacFadden, M. G. Leakey, J. Quade, V. Eisenmann *et al.*,
613   *Nature* **389**, 153 (1997/09/01, 1997).
614 89. M. Arakaki, P. A. Christin, R. Nyffeler, A. Lendel, U. Eggli, R. M. Ogburn *et al.*, *Proc Natl*
615   *Acad Sci U S A* **108**, 8379 (May 17, 2011).
616 90. T. J. Givnish, D. Spalink, M. Ames, S. P. Lyon, S. J. Hunter, A. Zuluaga *et al.*, *Proc. R. Soc.*
617   *B.* **282**, (2015).
618 91. E. J. Edwards, *New Phytologist* **223**, 1742 (2019/09/01, 2019).
619 92. J. R. Ehleringer, T. E. Cerling, B. R. Helliker, *Oecologia* **112**, 285 (1997/10/01, 1997).
620 93. H. Zhou, B. R. Helliker, M. Huber, A. Dicks, E. Akçay, *Proceedings of the National*
621   *Academy of Sciences* **115**, 12057 (2018/11/20, 2018).
622 94. C. E. R. Lehmann, S. A. Archibald, W. A. Hoffmann, W. J. Bond, *New Phytologist* **191**, 197
623   (2011/07/01, 2011).
624 95. W. M. Kürschner, Z. Kvacek, D. L. Dilcher, *Proceedings of the National Academy of*
625   *Sciences USA* **105**, 449 (2008).
626 96. C. A. E. Strömberg, *Annual Review of Earth and Planetary Sciences* **39**, 517 (2011/05/30,
627   2011).

628　97.　A. T. Karp, K. T. Uno, P. J. Polissar, K. H. Freeman, *Paleoceanography and*
629　　　　*Paleoclimatology* **36**, e2020PA004106 (2021/04/01, 2021).
630　98.　T. Kukla, J. K. C. Rugenstein, D. E. Ibarra, M. J. Winnick, C. A. E. Strömberg, C. P.
631　　　　Chamberlain, *AGU Advances* **3**, e2021AV000566 (2022/04/01, 2022).
632　99.　M. Fortelius, J. T. Eronen, F. Kaya, H. Tang, P. Raia, K. Puolamäki, *Annual Review of Earth*
633　　　　*and Planetary Sciences* **42**, 579 (2014/05/30, 2014).
634　100.　F. Kaya, F. Bibi, I. Žliobaitė, J. T. Eronen, T. Hui, M. Fortelius, *Nature Ecology & Evolution*
635　　　　**2**, 241 (2018/02/01, 2018).
636　101.　C. M. Janis, J. Damuth, J. M. Theodor, *Proceedings of the National Academy of Sciences*
637　　　　**97**, 7899 (2000).
638　102.　M. Fortelius, N. Solounias, *American Museum Novitates* **3301**, 1 (2000).
639　103.　M. C. Mihlbachler, F. Rivals, N. Solounias, G. M. Semprebon, *Science* **331**, 1178
640　　　　(2011/03/04, 2011).
641　104.　C. A. E. Strömberg, *Paleobiology* **32**, 236 (2006).
642　105.　C. M. Janis, M. Fortelius, *Biol Rev Camb Philos Soc* **63**, 197 (May, 1988).
643　106.　M. R. Badger, D. Hanson, G. D. Price, *Funct Plant Biol* **29**, 161 (Apr, 2002).
644　107.　M. P. S. Badger, *Biogeosciences* **18**, 1149 (2021).
645　108.　Y. G. Zhang, M. Pagani, Z. Liu, S. M. Bohaty, R. DeConto, *Philosophical Transactions of*
646　　　　*the Royal Society A: Mathematical, Physical and Engineering Sciences* **371**, (October 28,
647　　　　2013, 2013).
648　109.　P. D. Tortell, *Limnology and Oceanography* **45**, 744 (2000/05/01, 2000).
649　110.　C. T. Bolton, H. M. Stoll, *Nature* **500**, 558 (2013).
650　111.　M. N. Evans, S. E. Tolwinski-Ward, D. M. Thompson, K. J. Anchukaitis, *Quaternary*
651　　　　*Science Reviews* **76**, 16 (2013/09/15/, 2013).
652　112.　G. J. Bowen, B. Fischer-Femal, G. J. Reichart, A. Sluijs, C. H. Lear, *Clim. Past* **16**, 65 (2020).
653　113.　M. B. Osman, J. E. Tierney, J. Zhu, R. Tardif, G. J. Hakim, J. King *et al.*, *Nature* **599**, 239
654　　　　(2021/11/01, 2021).
655　114.　C. Godbillot, F. Minoletti, F. Bassinot, M. Hermoso, *Clim. Past* **18**, 449 (2022).
656　115.　A. Pack, A. Gehler, A. Süssenberger, *Geochimica et Cosmochimica Acta* **102**, 306
657　　　　(2013/02/01/, 2013).
658　116.　C. R. Scotese, *Annual Review of Earth and Planetary Sciences* **49**, 679 (2021/05/30,
659　　　　2021).
660　117.　P. A. Christin, C. P. Osborne, R. F. Sage, M. Arakaki, E. J. Edwards, *Journal of*
661　　　　*experimental Botany* **62**, 3171 (2011).
662

670

714   Funding acquisition: BH, PP, DLR, DOB, GJB, MJK, AP, RMdC, MH, KES, VF

715   Project administration: BH, DLR, DOB, PJP, GJB

716   Writing – original draft: BH, DLR, DOB, PJP, GJB, MJH, YC, MS, JCM, MJK, AP, KTU,
717   AR, SRP

718   Writing – review & editing: all

719

720   **Competing interests:** None.

721

722   **Data and materials availability:** The completed data sheets for each study can be accessed as the
723   paleo-CO$_2$ 'Archive' at NOAA's National Center for Environmental Information (NCEI). The
724   specific choice of category, as well as the updated CO$_2$ and age estimates, are documented in
725   'Product' sheets for each data set and proxy. In contrast to the 'Archive', which will grow with new
726   publications but will otherwise remain passive, the paleo-CO$_2$ 'Product' is a living database that
727   will be updated when newly published data or ancillary data constraints become available, and/or
728   methodological improvements are developed that enable modernization of previously
729   underconstrained datasets. The 'Product' sheets created for this study can be accessed in NCEI, and
730   this is also the place where future data updates will be made available in consecutive versions of
731   the data 'Product'.

732

733   **Authors composing the Consortium:**

734   Bärbel Hönisch[1*], Dana L. Royer[2*], Daniel O. Breecker[3*], Pratigya J. Polissar[4*], Gabriel J. Bowen[5*],
735   Michael J. Henehan[6], Ying Cui[7], Margret Steinthorsdottir[8], Jennifer C. McElwain[9], Matthew J.
736   Kohn[10], Ann Pearson[11], Samuel R. Phelps[12], Kevin T. Uno[1], Andy Ridgwell[13*], Eleni Anagnostou[14],
737   Jacqueline Austermann[1], Marcus P. S. Badger[15], Richard S. Barclay[16], Peter K. Bijl[17], Thomas B.
738   Chalk[18], Christopher R. Scotese[19], Elwyn de la Vega[20], Robert M. DeConto[21], Kelsey A. Dyez[22],
739   Vicki Ferrini[1], Peter J. Franks[23], Claudia F. Giulivi[1], Marcus Gutjahr[14], Dustin T. Harper[5], Laura L.
740   Haynes[24], Matthew Huber[25], Kathryn E. Snell[26], Benjamin A. Keisling[27], Wilfried Konrad[28], Tim K.
741   Lowenstein[29], Alberto Malinverno[1], Maxence Guillermic[30], Luz María Mejía[31], Joseph N.
742   Milligan[16], John J. Morton[1], Lee Nordt[32], Ross Whiteford[33], Anita Roth-Nebelsick[34], Jeremy K. C.
743   Rugenstein[35], Morgan F. Schaller[36], Nathan D. Sheldon[22], Sindia Sosdian[37], Elise B. Wilkes[38],
744   Caitlyn R. Witkowski[6], Yi Ge Zhang[39], Lloyd Anderson[1], David J. Beerling[40], Clara Bolton[18], Thure
745   E. Cerling[5], Jennifer M. Cotton[41], Jiawei Da[3], Douglas D. Ekart[42], Gavin L. Foster[**43**], David R.
746   Greenwood[44], Ethan G. Hyland[45], Elliot A. Jagniecki[46], John P. Jasper[47], Jennifer B. Kowalczyk[48],
747   Lutz Kunzmann[49], Wolfram M. Kürschner[50], Charles E. Lawrence[48], Caroline H. Lear[37], Miguel A.
748   Martínez-Botí[51], Daniel P. Maxbauer[52], Paolo Montagna[53], B. David A. Naafs[6], James W. B. Rae[33],
749   Markus Raitzsch[54], Gregory J. Retallack[55], Simon J. Ring[56], Osamu Seki[57], Julio Sepúlveda[26],
750   Ashish Sinha[58], Tekie F. Tesfamichael[59], Aradhna Tripati[30], Johan van der Burgh[60], Jimin Yu[61],
751   James C. Zachos[62], Laiming Zhang[63]

752

753

19

Affiliations:

Corresponding authors. Email: hoenisch@ldeo.columbia.edu, droyer@wesleyan.edu, breecker@jsg.utexas.edu, gabe.bowen@utah.edu, polissar@ucsc.edu, andy@seao2.org

[1] *Lamont-Doherty Earth Observatory of Columbia University, Palisades, United States*
[2] *Wesleyan University, Middletown, United States*
[3] *The University of Texas at Austin, Austin, United States*
[4] *University of California Santa Cruz, Santa Cruz, United States*
[5] *University of Utah, Salt Lake City, United States*
[6] *University of Bristol, Bristol, United Kingdom*
[7] *Montclair State University, Montclair, United States*
[8] *Swedish Museum of Natural History, Stockholm, Sweden*
[9] *Trinity College Dublin, Dublin, Ireland*
[10] *Boise State University, Boise, United States*
[11] *Harvard University, Cambridge, United States*
[12] *CIM Group, New York, United States*
[13] *University of California Riverside, Riverside, United States*
[14] *GEOMAR Helmholtz-Zentrum für Ozeanforschung Kiel, Germany*
[15] *The Open University, Milton Keynes, United Kingdom*
[16] *Smithsonian Institution, Washington, DC, United States*
[17] *Utrecht University, Utrecht, Netherlands*
[18] *Aix Marseille University, CNRS, IRD, INRAE, CEREGE, Aix-en-Provence, France*
[19] *Northwestern University, Evanston, United States*
[20] *University of Galway, Galway, Ireland*
[21] *University of Massachusetts, Amherst, United States*
[22] *University of Michigan, Ann Harbor, United States*
[23] *The University of Sydney, Sydney, Australia*
[24] *Vassar College, Poughkeepsie, United States*
[56] *Purdue University, West Lafayette, United States*
[26] *University of Colorado Boulder, Boulder, United States*
[27] *University of Texas Institute for Geophysics, Austin, United States*
[28] *University of Tübingen, Tübingen, Germany*
[29] *Binghamton University, Binghamton, United States*
[30] *University of California Los Angeles, Los Angeles, United States*
[31] *MARUM, University of Bremen, Bremen, Germany*
[32] *Baylor University, Waco, United States*
[33] *University of St Andrews, St Andrews, United Kingdom*
[34] *State Museum of Natural History, Stuttgart, Germany*
[35] *Colorado State University, Fort Collins, United States*
[36] *Rensselaer Polytechnic Institute, Troy, United States*
[37] *Cardiff University, Cardiff, United Kingdom*
[38] *Ginkgo Bioworks, Boston, United States*
[39] *Texas A&M University, College Station, United States*
[40] *University of Sheffield, Sheffield, United Kingdom*
[41] *California State University Northridge, Northridge, United States*
[42] *n/a, Salt Lake City, United States*

800   [43] *University of Southampton, Southampton, United Kingdom*

801   [45] *Department of Biology, Brandon University, Brandon, Canada*

802   [45] *North Carolina State University, Raleigh, United States*

803   [46] *Utah Geological Survey, Salt Lake City, United States*

804   [47] *Molecular Isotope Technologies, LLC, Niantic, United States*

805   [48] *Brown University, Providence, United States*

806   [49] *Senckenberg Natural History Collections, Dresden, Germany*

807   [50] *University of Oslo, Oslo, Norway*

808   [51] *EIT Urban Mobility, Barcelona, Spain*

809   [52] *Carleton College, Northfield, United States*

810   [53] *Institute of Polar Sciences - National Research Council, Bologna, Italy*

811   [54] *Dettmer Group KG, Bremen, Germany*

812   [55] *University of Oregon, Eugene, United States*

813   [56] *Deutsches GeoForschungsZentrum GFZ, Potsdsam, Germany*

814   [57] *Hokkaido University, Sapporo, Japan*

815   [58] *California State University Dominguez Hills, Carson, United States*

816   [59] *Addis Ababa University, Addis Ababa, Ethiopia*

817   [60] *n/a, Rossum, The Netherlands*

818   [61] *Laoshan Laboratory, Qingdao, China*

819   [62] *University of California Santa Cruz, Santa Cruz, United States*

820   [63] *China University of Geosciences, Beijing, China*

821

822 **List of Supplementary Materials**

823 Supplementary Text, Sections 1-10, Figs. S1 to S13

824 Tables S1 to S3

825 References (*118-439*)

826

827

828   **Figures :**

829   **Fig. 1. Documentation and assessment of all Cenozoic paleo-CO$_2$ estimates published to**
830   **date**. Individual proxy estimates are defined by colored symbols in legends. **(a)** Vetted Category
831   1 estimates with their fully developed uncertainty estimates (95% CIs); age uncertainties have
832   been updated or established to the best of current understanding. **(b)** Vetted Category 2 estimates
833   whose uncertainty is not yet fully constrained. Category 1 data are shown in grey for reference.
834   **(c)** Archive compilation of all CO$_2$ estimates in their originally published quantification. To
835   toggle view of individual proxy records in panels (a) and (c), please go to paleo-co2.org (Note:
836   panel (a) visualization will be published on the website after acceptance of the manuscript for
837   publication).

838
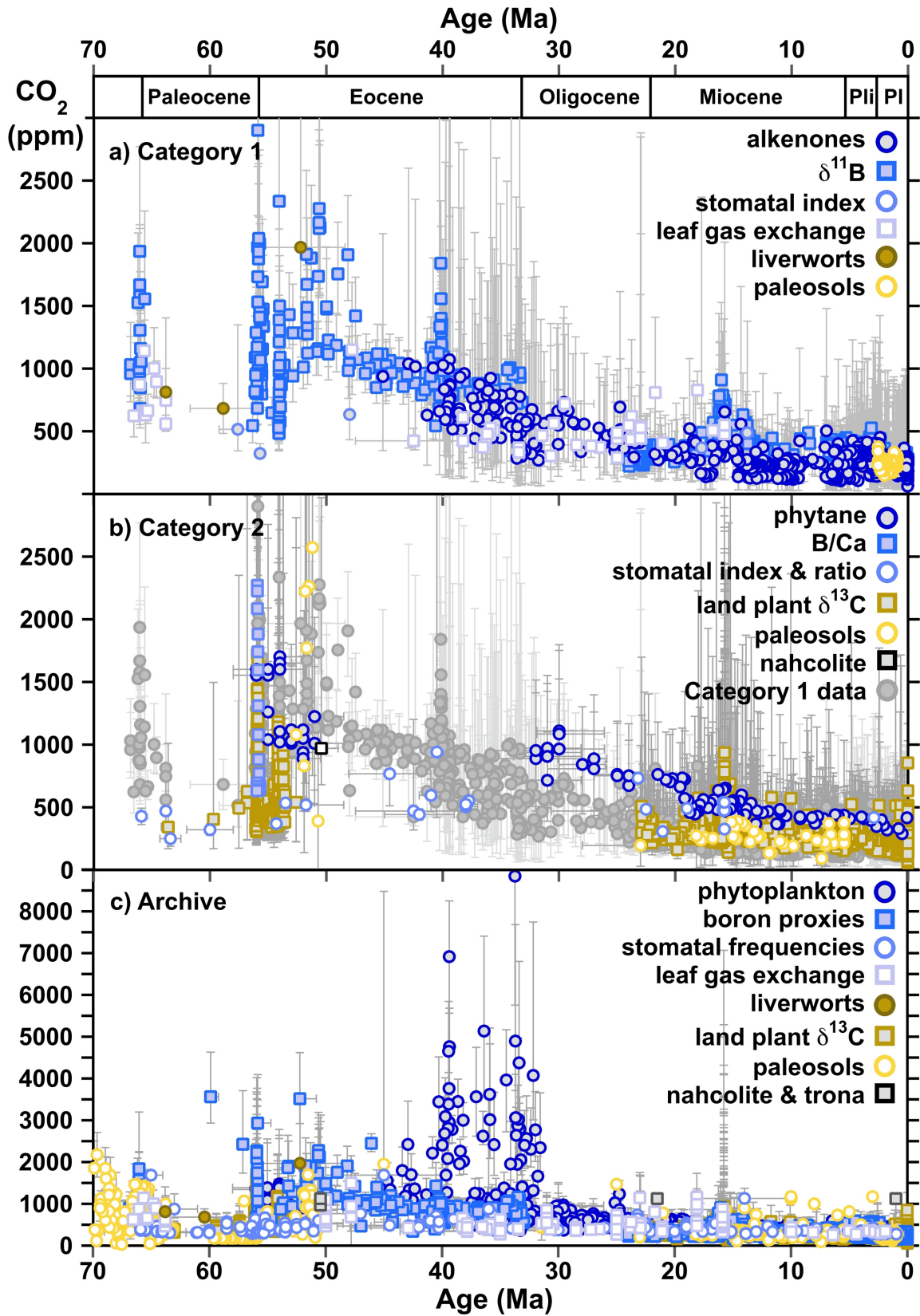
840 **Fig. 2. Category 1 paleo-CO₂ record compared to global climate signals.** The vertical dashed
841 line indicates the onset of continent-wide glaciation in Antarctica. **(a)** Atmospheric CO_2
842 estimates (symbols) and 500-kyr mean statistical reconstructions (median and 50 and 95%
843 credible intervals - dark and light-blue shading, respectively). Major climate events are
844 highlighted (K-PG - Cretaceous/Paleogene boundary, PETM - Paleocene Eocene Thermal
845 Maximum, EECO - Early Eocene Climatic Optimum, MECO - Middle Eocene Climatic
846 Optimum, EOT - Eocene/Oligocene Transition, MCO - Miocene Climatic Optimum, NHG -
847 onset of Northern Hemisphere Glaciation, MPT - Mid Pleistocene Transition). The 2022 annual
848 average atmospheric CO_2 of 419 ppm is indicated for reference. **(b)** Global mean surface
849 temperatures estimated from benthic $\delta^{18}O$ data after Westerhold et al. (*43*) (solid line, individual
850 proxy estimates as symbols, and statistically reconstructed 500-kyr mean values shown as the
851 continuous curve, with 50 and 95% credible intervals) and from surface temperature proxies (*45*)
852 (grey boxes). **(c)** Sea level after Ref. (*66*) with gray dots displaying raw data; the solid black line
853 reflects median sea level in a 1-Myr running window. High- and lowstands are defined within a
854 running 400-kyr window, with lower and upper bounds of highstands defined by the 75th and
855 95th percentiles, and lower and upper bounds of lowstands defined by the 5th and 25th
856 percentiles in each window. Globes depict select paleogeographic reconstructions and the
857 growing presence of ice sheets in polar latitudes from Ref. (*116*). **(d)** Crown ages show C₄
858 clades, with CCMs adapted to low CO_2, initially diversified in the early Miocene and then
859 rapidly radiated in the late Miocene (*117*). Flora transition from dominantly forested and
860 woodland to open grassland habitats based on fossil phytolith abundance data (*96*). North
861 American equids typify hoofed animal adaptations to new diet and environment (*103*), including
862 increasing tooth mesowear (black line, note inverted scale), hypsodonty (blue line), and body
863 size.

864
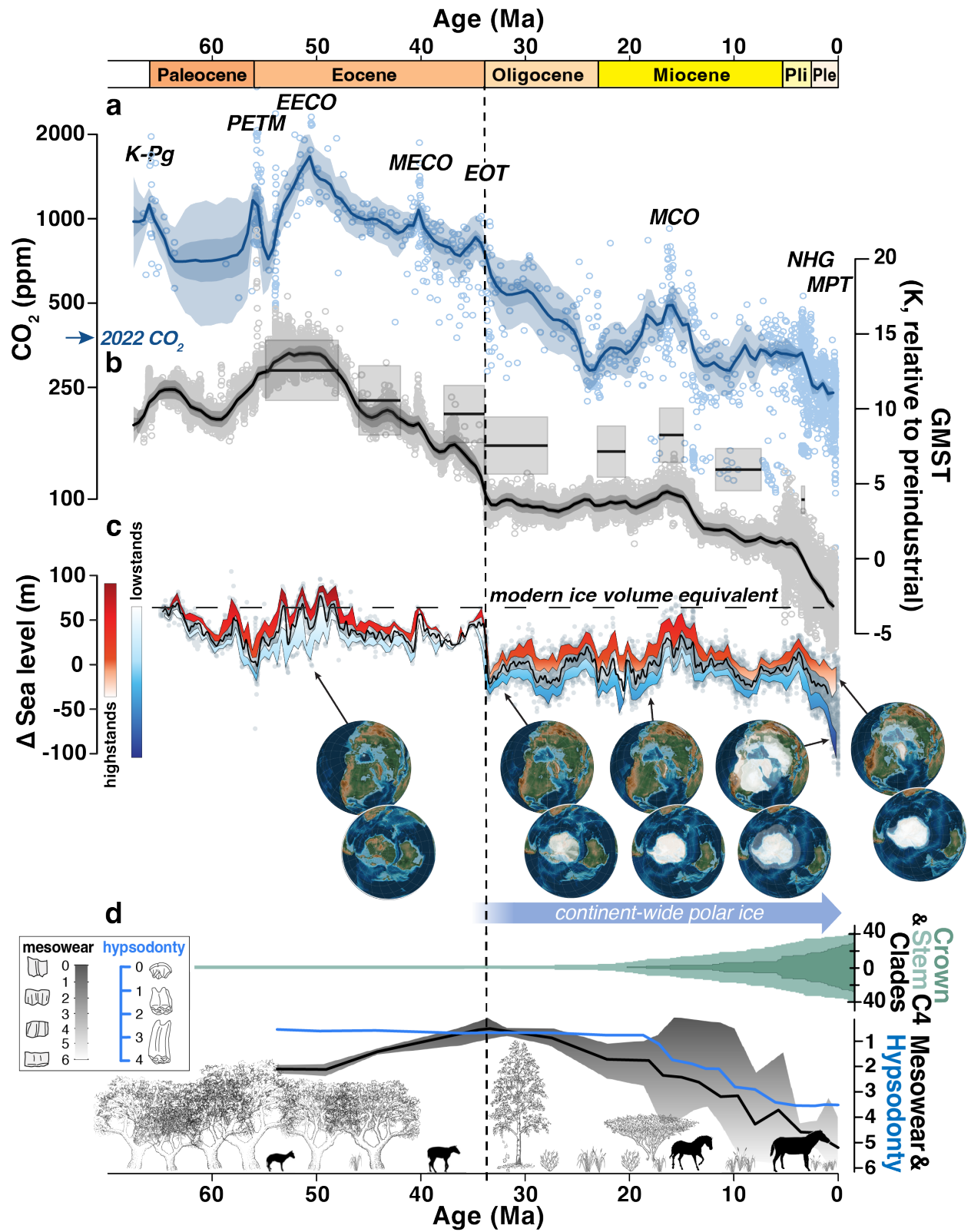
867   **Fig. 3. Application of the Category 1 CO_2 record to determine $ESS_{[CO2]}$.** GMST deviation
868   (K) from preindustrial global average surface temperature of 14.15°C is displayed versus paleo-
869   CO_2 doublings relative to the preindustrial baseline of 280 ppm (upper x-axis) and paleo-CO_2
870   estimates on a log scale (lower x-axis). The slopes between two points in time reflect the average
871     $ESS_{[CO2]}$. Circles reflect 500-kyr binned 'Category 1' CO_2 estimates paired with corresponding
872   GMST-means from Ref. (*43*), squares pair CO_2 and GMST means from compilations of sea
873   surface temperature (*45*) in seven coarsely resolved time intervals. Note that this figure omits the
874   Pliocene temperature estimate of (*45*) because it samples too short a time interval (cf. Fig. 2) to
875   be comparable with mean CO_2. Data from Cenozoic epochs are color coded and shift from red
876   (Paleocene) to yellow (Pleistocene); labels indicate specific age bins (Ma). Dashed lines indicate
877   reference $ESS_{[CO2]}$ lines of 8 and 5°C warming per doubling of CO_2.
878